ELSEVIER

Chemical Physics 239 (1998) 187–197

Chemical Physics

Effects of complex formation on reactions of oxygen with HCl and Ar–HCl

Michael W. Lufaso, Anne B. McCoy [1]

Department of Chemistry, The Ohio State University, Columbus, OH 43210, USA

Received 18 May 1998

Abstract

Classical trajectory simulations are used to investigate reactions of HCl and Ar–HCl with atomic oxygen in its ground and first excited states. We focus on the effects of complex formation on reaction cross sections and product state distributions over a range of collision energies. At low collision energies, the argon atom inhibits the formation of the H–O–Cl collision complex and lowers the reaction cross sections. At higher collision energies, the argon atom removes energy from the collision complex, thereby lowering the effective collision energy and increasing the cross sections for reaction. In general, the product state distributions, resulting from reactions of complexes, are shifted to lower energies than the product state distributions of corresponding O + HCl reactions. © 1998 Elsevier Science B.V. All rights reserved.

1. Introduction

Over the past twenty-five years, experimental and theoretical approaches have been developed to the point that a variety of atom plus diatom (A + BC) reactions have been mapped out very accurately [1–3]. While much can be learned from these studies most chemistry, in the laboratory and in nature, is more complicated. For example, the reactants and products usually contain more than three atoms, often more than two molecules are involved in the reaction and typically reactions take place in the presence of other, chemically inert, molecules rather than in vacuum. If we can understand how the evolution of a simple system from reactants to products is affected by interactions with even one chemically inert moiety we will have achieved an important first step in the overall goal of understanding how solvation affects chemical reaction dynamics.

Laboratory studies have demonstrated that the incorporation of one or both of the reactants of a gas phase reaction in a cluster can change the products for that reaction [4,5]. For example, putting the reactants into a cluster can facilitate an otherwise forbidden process, as is the case for low energy collisions of $O(^3P)$ and HCl [6] and in methane activation by $Rh_n^+Ar_m$ clusters [7] or it can close a reactive pathway, as in the electronic predissociation of $HS(A^2\Sigma^+)$ in Ar–HS complexes [8–10]. Changes in the rates of important atmospheric processes by incorporation of at least one of the reactants into a cluster can have a profound impact on the predicted chemistry [11].

In the present study we use classical trajectory simulations to investigate the effect of complex for-

[1] Corresponding author.

0301-0104/98/$ - see front matter © 1998 Elsevier Science B.V. All rights reserved.
PII: S0301-0104(98)00277-8

mation on the dynamics and product state distributions of the reactions:

$$O(^1D) + HCl \rightarrow OH(^2\Pi) + Cl(^2P) \quad (R1)$$

$$\rightarrow OCl(^2\Pi) + H(^2S) \quad (R2)$$

$$O(^3P) + HCl \rightarrow OH(^2\Pi) + Cl(^2P) \quad (R3)$$

over a range of collision energies. In previously reported classical studies of these reactions at 1 eV collision energies, we found that in reactions (R2) and (R3) complexing HCl with one argon atom led to less angular momentum in the diatomic product. In contrast, the vibrational and angular momentum distributions of the OH formed by reaction (R1) were not affected by the presence of an argon atom [12]. These results were rationalized in terms of the relative lifetimes of the H–O–Cl collision complex and the van der Waals complex. The shorter lived the van der waals complex, relative to the lifetime of the collision complex, the smaller the effects of complexation on the angular momentum and vibrational energy distributions. The lifetimes can, in turn, be related to the energetics of the reactions, displayed in Fig. 1. These plots are based on the $O(^3P) + HCl$ potential of Koizumi, Schatz and Gordon [13] and the $O(^1D) + HCl$ potential of Schinke [14]. According to these potentials, reaction (R1) is exothermic by 2 eV, with a strongly bound HOCl complex, while reaction (R2) is endothermic by 0.3 eV and may proceed either by going through the HOCl complex or by forming a H–Cl–O collision complex, which is 1 eV higher in energy than the reactants. Finally, reaction (R3) is thermoneutral and has a barrier of approximately 0.45 eV.

It should be noted that there is some uncertainty the correct barrier height for reaction (R3) [15,16,13] and reaction (R2) should be slightly exothermic [14,17], but given the differences in the energetics of reactions (R1)–(R3), they provide a laboratory in which classical mechanics can be used to investigate some of the effects of complex formation on reaction dynamics. By comparing the results for reactions of HCl and Ar–HCl, we can begin to map out ways in which the introduction of a single chemically inert species alters the reaction dynamics and product state distributions.

The remainder of the paper is organized as follows. In Section 2, we describe the classical trajectory simulations and potential energy surfaces used in this study. The reaction cross sections and product state distributions for reactions (R1)–(R3) are presented and the effects of collision energy on these quantities is discussed in Section 3. Finally, the results are summarized and conclusions are drawn in Section 4.

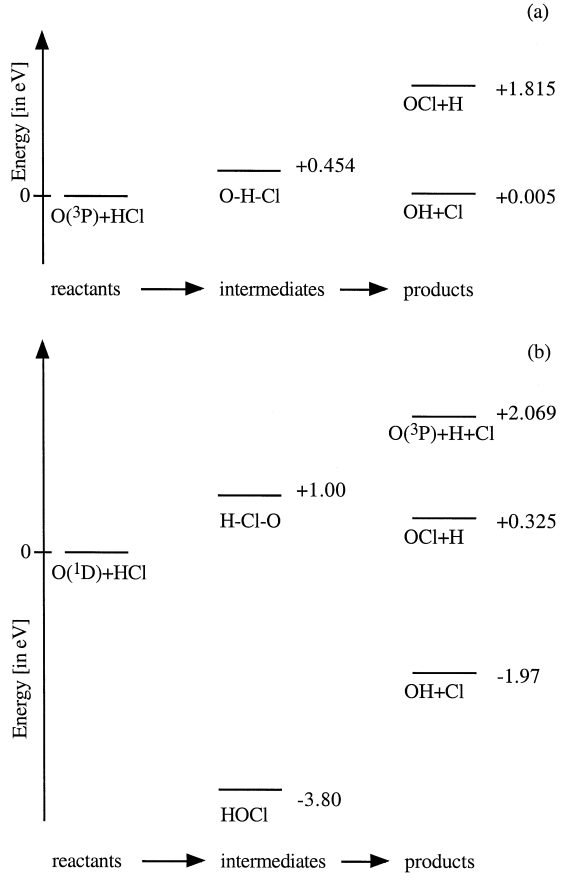

Fig. 1. The energetics of the reactions of (a) $O(^3P)$ and (b) $O(^1D)$ with HCl. The reported energies are based on the Koiozumi, Schatz and Gordon [13] and Schinke [14], potentials, respectively. All energies are reported in eV the energy of the reactants define the zero in energy.

2. Methods

In this study, we employ quasi-classical [18,19] trajectory simulations to investigate the dynamics of

collisions of atomic oxygen and HCl. Classical approaches have long been recognized to display serious deficiencies when used to describe hydride transfer reactions [20,21]. In particular they cannot properly treat tunneling or zero-point effects. Here we will focus on relatively high collision energies, 1–3.5 eV for the $O(^3P)$ + HCl reactions and 0.25–3.5 eV for the $O(^1D)$ + HCl reactions, where classical approaches can be expected to provide a reasonable description of the dynamics [20].

2.1. Initial conditions

We initiate the oxygen + Ar–HCl trajectories with Ar–HCl in its ground rotation/vibration state. This is achieved by running a long time, 500 ps, trajectory of Ar–HCl with HCl in its equilibrium configuration and zero-point energy in the intermolecular vibrational modes so that the total energy of the system is 57 cm^{-1} above the Ar–HCl minimum. For these simulations, the H6(3) potential of Hutson is used [22]. Because the potential does not include any explicit couplings between the HCl vibrational motions and the intermolecular motions and because the kinetic coupling is weak, the zero-point energy remains localized in the intermolecular motions over these propagation times.

The initial Ar–HCl coordinates and momenta are randomly sampled from this long time trajectory. This ensures reasonable sampling of the relevant Ar–HCl geometries. The HCl bond length is then increased from the equilibrium value to 1.4022 Å in order to put zero-point energy in this mode as well. Since the HCl vibrations are fast, the results should not be sensitive to the initial phase of the vibration. Further, because the trajectories are run for less than 300 fs prior to the collision with the oxygen atom, we do not expect there will be significant leakage of zero-point energy from the HCl vibration into the intermolecular modes of the system. Once a collision occurs, the total available energy is at least forty times the binding energy of the van der Waals complex and it is not expected to survive a collision.

The initial distance between the oxygen atom and the center of mass of the Ar–HCl complex is 10 Å. The impact parameter b and three Euler angles that describe the orientation of the Ar–HCl are drawn from random distributions. Here we select the angles ϕ and η from a uniform distribution on $(0,2\pi)$. The third angle θ, which provides the angle between the relative velocity vector of the oxygen atom and the vector that describes the location of the argon atom relative to the center of mass of HCl, is sampled from the probability distribution:

$$P(\theta) = \frac{\theta}{\sin\theta}\left[1 - \left(\frac{\theta}{\pi}\right)^2\right], \tag{4}$$

or $\theta = \pi\left[1 - (1-\xi)^{1/2}\right]$, where ξ is selected from a uniform random distribution on (0,1). Finally, the impact parameter b is taken from the distribution:

$$P(b) = \left[1 - \left(\frac{b}{b_{max}}\right)^2\right], \tag{5}$$

or $b = b_{max}\left[1 - (1-\xi)^{1/2}\right]^{1/2}$, where b_{max} is the maximum value of the impact parameter used in the study, the values of which are provided in Table 1. The above choices of $P(\theta)$ and $P(b)$ ensure that collisions with small impact parameters and near colinear O–Ar–HCl geometries are favored, but weighted appropriately.

Reactions without the argon atom are also studied, for comparison. The same set of initial conditions are used in both ensembles of trajectories although here b,θ and ϕ are measured relative to the center of mass of HCl rather than Ar–HCl. The product state distributions for these reactions have been found to be sensitive to the rotational temperature of the HCl reactants [14]. To facilitate the comparison, we use the same initial angular momentum for HCl as is used for the Ar–HCl trajectories.

2.2. Propagations

The potentials that describe the reactions of oxygen with HCl or Ar–HCl are approximated by the sum of the O + HCl [13,14], ArH [23], ArO [24] and ArCl [25] potentials which were previously fit to *ab initio* and empirical data. These potentials have been described in detail elsewhere [12]. While they do not

Table 1
Cross sections for products of O + HCl and Ar–HCl reactions. Unless otherwise noted, all runs are based on 10 000 trajectories with $b_{max} = 7.94$ Å

Reaction	E_{trans} [a]	σ_{OH} [b]	σ_{OCl}	σ_{HOCl}
$O(^3P)$ + HCl	1.00 [c]	0.143(0.017)	–	–
	2.00 [c]	0.185(0.036)	–	–
	3.28 [d,e]	0.084(0.006)	0.003(0.000)	–
$O(^3P)$ + Ar–HCl	1.00 [c,d]	0.106(0.014)	–	–
	2.00 [c]	0.562(0.045)	–	–
	3.28 [c]	0.745(0.048)	0.004(0.001)	–
$O(^1D)$ + HCl	0.25	15.39(0.38)	0.269(0.053)	–
	0.50	11.45(0.33)	0.638(0.087)	–
	0.75	10.92(0.32)	0.700(0.087)	–
	1.00 [c]	10.23(0.15)	0.392(0.034)	–
	1.50 [c]	7.56(0.14)	0.392(0.034)	–
	1.75 [c]	6.58(0.13)	0.389(0.034)	–
	2.00 [c]	6.25(0.13)	0.356(0.031)	–
	3.28 [c]	5.28(0.12)	0.132(0.020)	–
$O(^1D)$ + Ar–HCl	0.25	12.74(0.36)	0.050(0.022)	–
	0.50	11.34(0.34)	0.532(0.076)	0.669(0.090)
	0.75	10.79(0.34)	0.734(0.090)	0.406(0.067)
	1.00	9.85(0.20)	0.605(0.048) [c]	0.347(0.045)
	1.50 [e]	9.59(0.22)	0.528(0.050)	0.202(0.034)
	1.75 [e]	8.62(0.22)	0.591(0.056)	0.182(0.031)
	2.00	7.50(0.28)	0.602(0.048) [c]	0.134(0.039)
	3.28 [c]	7.26(0.18)	0.384(0.036)	0.025(0.000)

[a] Collision energy in eV
[b] Given in $Å^{-2}$ with one standard deviation given in parentheses.
[c] Based on a b_{max} of 3.97 Å.
[d] Based on 20 000 trajectories.
[e] Based on a b_{max} of 1.99 Å.
[f] Based on a b_{max} of 5.29 Å.

reproduce the well-known Ar–OH [26] or Ar–HCl [22] van der Waals interactions, we have shown that they provide a good qualitative description and have the advantage that they generate an intermolecular potential that is smooth everywhere [12]. Although two electronic states of oxygen are considered in this study, the $O(^1D)$ surface of Schinke [14], and the $O(^3P)$ surface of Koiozumi and coworkers, all propagations are run on a single O + HCl potential surface and crossing between the $O(^1D)$ and $O(^3P)$ surfaces is not included in the simulations. Finally, the trajectories are run using a Gear, predictor/corrector propagator [27].

2.3. Analysis of the results

From the outcomes of the trajectories, we can classify the products into one of four general channels, depending on the relative bond lengths:

$$\begin{aligned} O + HCl &\rightarrow O + HCl^* \\ &\rightarrow OH + Cl \\ &\rightarrow OCl + H \\ &\rightarrow HOCl \end{aligned}$$

where the $*$ on the HCl product is used to indicate vibrational excitation. The HOCl product is said to be formed when the average of the HCl, OCl and OH distances is smaller than 2.65 Å at the end of the propagation. If the distance between the argon atom and the center of mass of either of the two products is smaller than 4.25 Å, that product is taken to be in a complex with argon. These represent metastable states that will eventually dissociate.

The results are analyzed in terms of the relative cross sections. We evaluate the cross sections for product channel α from:

$$\sigma_\alpha = \frac{1}{N} \sum_{i=1}^{N_\alpha}{}' w_i \tag{6}$$

where N is the total number of trajectories run, typically 10 000 and, based on the distributions in Eqs. (4) and (5),

$$w_i = \frac{\pi}{16} \frac{\pi^4 \sin(\theta_i)}{\theta_i(\pi^2 - \theta_i^2)} \frac{b_{max}^4}{b_{max}^2 - b_i^2}. \tag{7}$$

The prime on the summation in Eq. (6) is used to emphasize that this sum is over only the N_α trajectories that end up in product channel α. All other distributions, e.g. lifetimes, vibrational energy, angular momentum, are calculated in terms of the relative cross section:

$$P(a) = \frac{1}{N\sigma_\alpha} \sum_{i=1}^{N_\alpha}{}' a_i w_i. \tag{8}$$

3. Results and discussion

3.1. $O(^1D) + HCl \rightarrow OH + Cl$

3.1.1. Cross sections

As is shown in Fig. 1, this reaction is exothermic by approximately 2 eV and proceeds through the

formation of a strongly bound HOCl complex. Given the energetics of this reaction, we expect that the cross section will decay approximately exponentially with collision energy [28]. The calculated cross sections for eight collision energies between 0.25 and 3.5 eV are reported in Table 1 and plotted with open squares in Fig. 2. We fit these points to the excitation function,

$$\sigma(E) = C\,e^{-mE}, \tag{9}$$

with $C = 15.81$ Å^2 and $m = 0.465$ eV^{-1}. The function also reproduces the cross sections reported by Schinke [14], plotted with diamonds in Fig. 2. The cross sections for OH formation from reactions of O(^{1}D) with Ar–HCl are plotted with filled squares. These were also fit to Eq. (9), with $C = 12.70$ Å^2 and $m = 0.214$ eV^{-1}.

An interesting feature of the cross sections for these reactions is that while at lower collision energies the cross section for the reaction with Ar–HCl, σ_{OH}^{Ar-HCl}, is smaller than that for reactions of HCl, σ_{OH}^{HCl}, at higher energies, $\sigma_{OH}^{Ar-HCl} > \sigma_{OH}^{HCl}$. To understand the observed trends, we need to consider three effects of the argon atom to the system. First, the introduction of the argon atom increases the effective size of the complex. This can be seen by comparing the two panels of Fig. 3, where the potential energy felt by the O(^{1}D) atom is plotted when (a) HCl and (b) Ar–HCl are in their equilibrium configurations. As can be seen by comparing the dotted contours at $-11\,500$ cm^{-1}, the Ar–HCl complex is more than twice the size of HCl. This increase in size should increase the cross section. One must also consider the fact that the argon atom will remove a fraction of the collision energy from the collision complex. For this reaction, we find that, on average, the argon atom leaves with 15 to 20% of the initial relative translational energy. This will lower the energy available for the O + HCl reaction, having a similar effect as lowering the collision energy. Since, according to Eq. (9), the cross section decreases with increasing collision energy, this effect

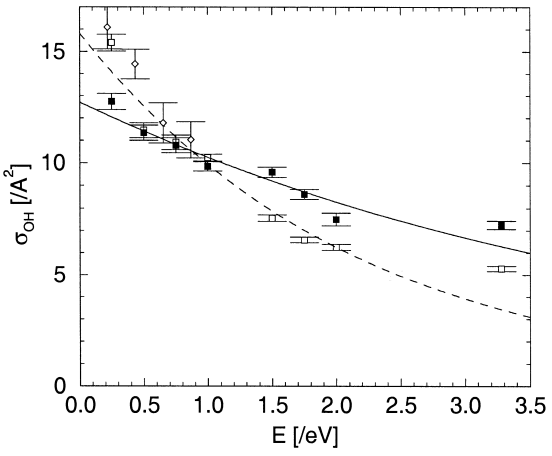

Fig. 2. The cross sections for OH formation from the reaction of O(^{1}D) with HCl and Ar–HCl. Results for collisions of HCl are represented by □ (present work) and ◇ (Ref. [13]). Reactions with Ar–HCl are shown with ■. The two data sets were fit to excitation functions, described in the text. All error bars represent an uncertainty corresponding to one standard deviation.

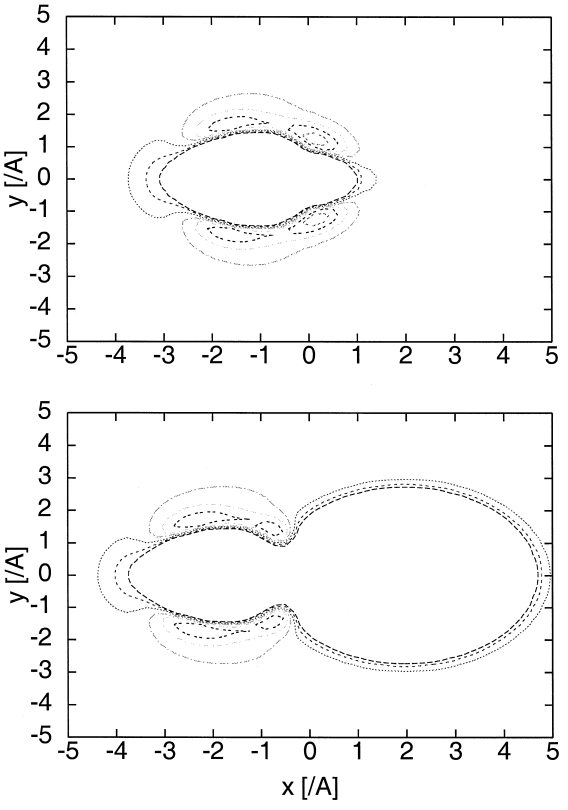

Fig. 3. Contour plots of the potential felt by O(^{1}D) in the presence of (a) HCl and (b) Ar–HCl in their equilibrium configurations. In both plots, the hydrogen atom is located at the origin, chlorine on the $-x$ axis and, in the lower panel, argon is on the $+x$ axis. The maximum energy contour is at $-10\,000$ cm^{-1} and contours are plotted in increments of 2500 cm^{-1}.

will also lead to an increase of σ_{OH}^{Ar-HCl}, compared to σ_{OH}^{HCl}. Finally, the argon atom can block the formation of the collision complex. This effect can be seen by comparing the size and depths of the wells on the hydrogen end of the HCl molecule in Fig. 3. When zero-point energy in the Ar–HCl bend is considered, the argon atom may completely block one of these wells, inhibiting complex formation and lowering the cross section.

Given the observed relative trends in σ_{OH}^{HCl} and σ_{OH}^{Ar-HCl}, we believe that the steric effects represent the dominant effect of the introduction of an argon atom when the collision energy is low. At the highest collision energies, we find that

$$\sigma_{OH}^{HCl}(E) \approx \sigma_{OH}^{Ar-HCl}(E - \langle E_{Ar} \rangle) \quad (10)$$

where $\langle E_{Ar} \rangle$ is the average kinetic energy of the argon atom for these collisions. This leads us to conclude that the energetic effect of the argon atom is more important than the size effect for this particular reaction. Similar behavior has been observed by Varandas and co-workers in their studies of reactions of H with Ar–O_2 [29].

3.1.2. OH product state distributions

Next we investigate the vibrational and angular momentum distributions of the OH products, plotted in Fig. 4 for collision energies of 0.5, 1.0 and 2.0 eV. In classical mechanics, vibrational energy and angular momentum are continuous, whereas in quantum mechanics energy and angular momentum are both quantized. Quantum number assignments are made for the diatomic product in each classical trajectory by determining the quantum state that is closest in energy and angular momentum to the classical values. The sums of the cross sections of all trajectories that result in the formation of OH in the same quantum state are plotted in Fig. 4. As can be seen in the plots in the left panels of Fig. 4, these distributions are nearly identical for the 0.5 eV collision energies and are shifted by approximately one quantum of vibrational energy for the 1 and 2 eV collisions. The observed shift of the vibrational energy distributions of the OH products that are formed when HCl is complexed with an argon atom results from approximately 15–20% of the collision energy being expressed as kinetic energy of the departing

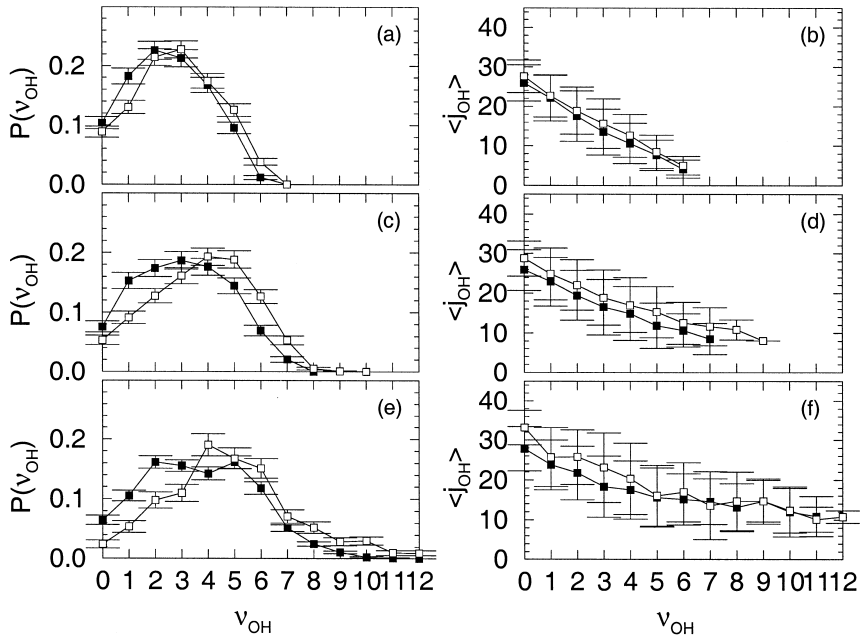

Fig. 4. Relative cross sections for the OH products of the $O(^1D)$ + HCl (□) and Ar–HCl (■) reactions at 0.5 eV [(a) and (b)]; 1 eV [(c) and (d)] and 2 eV [(e) and (f)] collision energies. The left column provides the vibrational distributions and the panels on the right give the angular momentum distributions, described in the text.

argon atom leaving less energy to the OH vibration. While for a 0.5 eV collision energy, this corresponds to a loss of 900 cm^{-1}($\approx \omega_{OH}/3$), at 2.0 eV collision energy the argon atom leaves with, on average, 2850 cm^{-1}.

In panels (b), (d) and (f) of Fig. 4, we compare the rotational distributions of the OH products. To condense the information, we have plotted $\langle j \rangle(\nu_{OH})$ as a function of ν_{OH}, and the error bars, δ, provides the widths of the angular momentum distributions,

$$\delta = \sqrt{\langle j^2 \rangle - \langle j \rangle^2} \ . \tag{11}$$

To aid the reader in understanding this notation, in Fig. 5, we have plotted the full rotational distributions for the 0.5 eV collisions when $\nu_{OH} = 1,3,5$. For $\nu_{OH} = 1$ and 5, the two rotational distributions are nearly identical, within their uncertainties. This leads to the exact overlap of these two points and their error bars in Fig. 4(b). In contrast, for $\nu_{OH} = 3$, the center of the rotational distribution for the reaction with Ar–HCl is shifted to lower j_{OH} and the distribution is slightly narrower.

The summarized results, plotted in Fig. 4, show that for lower collision energies, the angular momentum distributions are not significantly affected by the introduction of an argon atom, but when we increase the collision energy, the rotational distributions that correspond to $\nu_{OH} \leq 5$ are cooler and narrower for the collisions with Ar–HCl. As with the vibrational distributions, this shift can be rationalized in terms of the increase in the magnitude of the average kinetic energy of the departing argon atom as the collision energy increases. Finally, the angular momentum distributions, plotted in Fig. 5, tend to become narrower and move to lower values of j_{OH}. In Fig. 4,

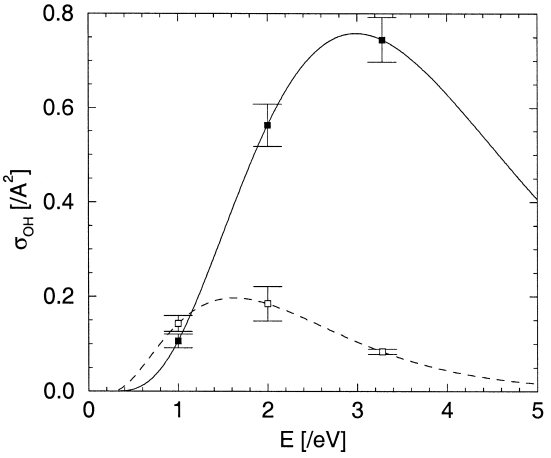

Fig. 6. Same as Fig. 2, but for the reaction of $O(^3P)$ with HCl and Ar–HCl.

this is represented by the negative slope of the $\langle j_{OH} \rangle$ versus ν_{OH} plots and in the decrease in δ with increasing ν_{OH}.

3.2. $O(^3P) + HCl \rightarrow OH + Cl$

3.2.1. Cross sections

In contrast to the $O(^1D) + HCl$ reaction, described above, the $O(^3P) + HCl \rightarrow OH + Cl$ reaction is approximately thermoneutral with a barrier of 0.45 eV, and the reaction is classically forbidden for collision energies below 0.45 eV. As such, the excitation function is expected to take the form [28]:

$$\sigma(E) = C(E - E_{th})^n e^{-m(E - E_{th})}. \tag{12}$$

The cross sections for this reaction are given in Table 1 and are plotted in Fig. 6. The curves are given by Eq. (12) with E_{th} taken to be the difference

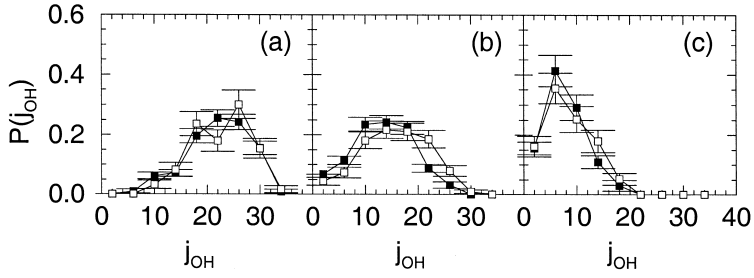

Fig. 5. Angular momentum distributions of the OH products that correspond to $\nu_{OH} =$ (a) 1; (b) 3 and (c) 5 for 0.5 eV collisions of $O(^1D)$ + HCl (□) and Ar–HCl (■).

between the barrier height and the zero-point energy of HCl, and C, m and n are chosen to reproduce the three values of $\sigma_{OH}(E)$ given in Table 1. Clearly with as many parameters as data points, we have no way to check the reliability of the parameters in Eq. (12), but we can investigate general features of the two curves.

As in the $O(^1D) + HCl$ reaction, at low collision energies $\sigma_{OH}^{HCl} > \sigma_{OH}^{Ar-HCl}$, while at higher energies $\sigma_{OH}^{Ar--HCl}$ is larger. We can invoke the three effects of the argon atom, described above. For low collision energies, steric effects appear to dominate. This is not surprising because the transition state for this reaction corresponds to a 135° O–H–Cl angle, whereas the minimum energy geometry of Ar–HCl has a 180° Ar–H–Cl angle. This puts the argon atom at a favorable position to block access to the transition state. Since the cross section for OH formation is as much as four times larger for collisions with Ar–HCl than with HCl, we conclude that at higher collision energies the increase in the size of the HCl complex is an important factor in the increase in the cross section. Finally, the shift in the peak in the excitation function can be attributed to the loss of, on average, 10% of the collision energy to translation of the argon atom.

3.2.2. OH product state distributions

Comparison of the vibrational and angular momentum distributions, plotted in Fig. 7, shows that the vibrational energies are colder by approximately one quantum and the angular momentum distributions are, in general, broader and colder for the reactions with Ar–HCl. The effect becomes more pronounced at higher collision energies. In these reactions, there are two effects that are leading to the cooler rotational distribution from the reaction with Ar–HCl. First, the argon atom will remove kinetic energy from the O–H–Cl system, thereby reducing the total energy available to the OH products. This mechanism tends to reduce the energy that is expressed both in rotation and vibration of the diatomic product. The second mechanism comes from the fact that there is a barrier to the reaction. Therefore, for low to moderate collision energies, the OH and chlorine atom are separating faster than the OH and

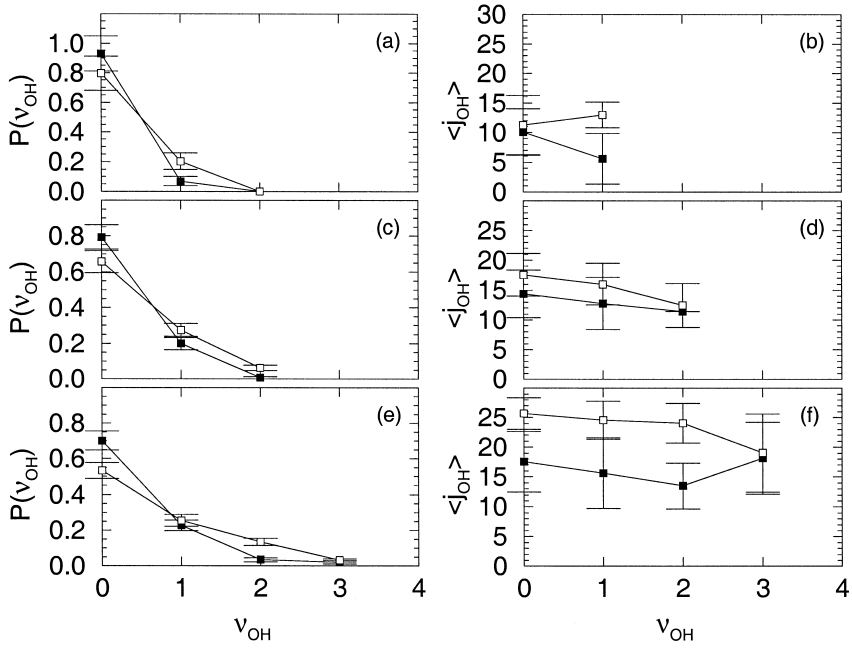

Fig. 7. Product state distributions for the OH products of the $O(^3P) + HCl$ (□) and Ar–HCl (■) reactions at 1 eV [(a) and (b)] and 2 eV [(c) and (d)] collision energies. The left column provides the vibrational energy distributions and the panels on the right give the angular momentum distributions, described in the text.

argon atom. As a result, energy can be transferred from the rotation of the OH product to translation of the argon atom. The effectiveness of this second mechanism will decrease with increasing total energy as the higher the collision energy the faster the complex will fall apart and the smaller the time over which energy can be transferred. Therefore, while at lower collision energies, the OH product has statistically less energy in rotation and vibration than in translation, at larger collision energies the vibrational energy and angular momentum distributions approach the statistical limit.

3.3. $O(^1D) + HCl \rightarrow OCl + H$

3.3.1. Cross sections

Finally we investigate the effects of the introduction of an argon atom to reaction (R2). This reaction is complicated by the fact that at low collision energies the reaction proceeds through the strongly bound HOCl complex, but, in contrast to the OH product channel, is endothermic by approximately 0.325 eV. When the system is initiated with 1.0 eV of excess energy a second channel is opened in which an H–Cl–O transition state complex is formed. In Table 1, we report the cross sections for this reaction at 8 collision energies. We find that these cross sections can be modeled by a pair of excitation functions of the form of Eq. (12) with $E_{th} = 0.325$ and 1.0 eV. These functions and the cross sections are plotted in Fig. 8. As in the $O(^3P) + HCl$ reaction, the number of parameters barely exceeds the number of calculated cross sections and we use these models only to make qualitative comparisons between the trends in the cross sections for the reactions with HCl and Ar–HCl.

Comparing the results for HCl and Ar–HCl, we find that at low collision energies, the differences can be accounted for by recognizing that, on average, 15% of the difference between the collision energy and the endothermicity of the reaction is expressed as translational energy of the argon atom. In other words,

$$\sigma_{OCl}^{HCl}(E) \approx \sigma_{OCl}^{Ar-HCl}(E - \langle E_{Ar} \rangle). \quad (13)$$

The differences in the higher energy excitation function are due to two factors. First, as in the $O(^3P) + HCl$ reaction, the increased size of the collision

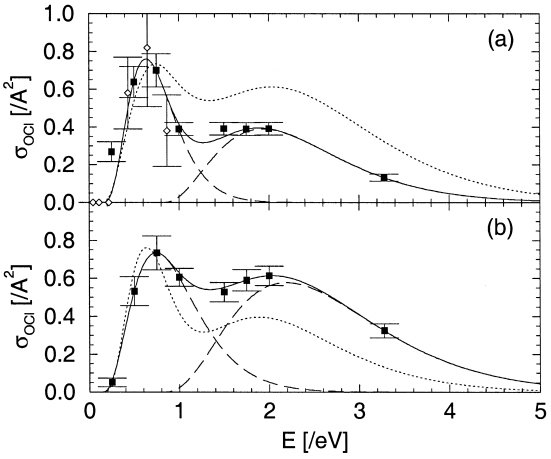

Fig. 8. The cross sections for OCl formation from the reaction of $O(^1D)$ with (a) HCl and (b) Ar–HCl. Results of the present work are represented by ■ and ◇ provide the results reported in Ref. [13]. The two data sets were fit to the sum of two excitation functions, as described in the text, where the dashed lines provide the two contributions that add to give the excitation function, plotted with a solid line. To facilitate comparison, the excitation functions for the O + Ar–HCl and O + HCl reactions are plotted with a dotted lines in (a) and (b), respectively.

partner may lead to a larger collision probability. In addition, for collision energies above 2 eV, the system has sufficient energy to dissociate into O + Cl + H. For these energies, the loss of kinetic energy to the argon atom effectively closes this reaction pathway, thereby significantly increasing the cross section for OCl formation.

3.3.2. OCl product state distributions

In Fig. 9, we plot the product state distributions for this reaction. At lower collision energies, the vibrational distributions are only slightly affected by the introduction of the argon atom, similar to the vibrational energy distributions for the OH products of these collisions. In contrast, here the angular momentum distributions of the OCl products are broadened and shifted to lower j_{OCl}.

The observed distributions can be rationalized in terms of the dynamics of this reaction. At lower collision energies, $E \leq 1$ eV, only the endothermic channel is opened. Therefore, in order to form OCl, most of the available energy must go into the H–OCl dissociation coordinate. This will result in very cold vibrational distributions. Since the argon atom re-

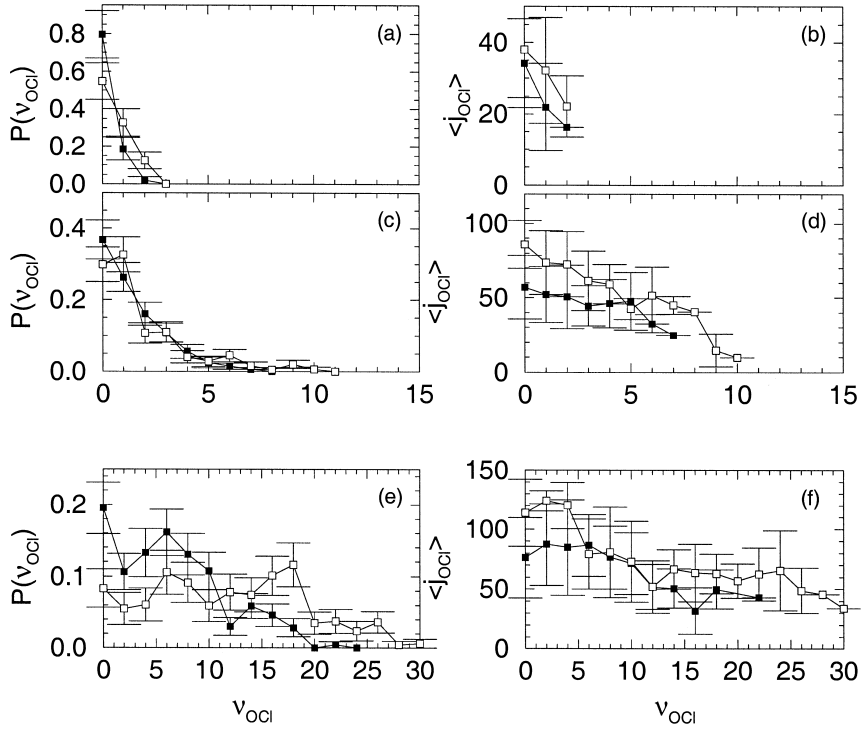

Fig. 9. Same as Fig. 4, but for the OCl products.

moves, on average, 15% of the excess energy, both the vibrational and rotational energy distributions will be colder when an argon atom is present and because the reaction proceeds through a strongly bound complex the energy is distributed statistically. The width of the OCl rotational distributions can be seen to result from the width in the velocity distribution of the departing argon atom.

At higher collision energies, the direct channel, in which the reaction proceeds over a H–O–Cl transition state, is also energetically accessible. This leads to the more complicated vibrational and rotational energy distributions, and, because some of the collision energy will be released as translational energy of the argon atom, the reactions that proceed through complex formation will be more important in the reactions of Ar–HCl.

4. Summary and conclusions

In this paper, we have investigated the effects of complexation with a single argon atom on the dynamics of reactions of atomic oxygen and HCl. Focusing on the reaction cross sections, we find that for the collisions that form OH, at lower collision energies, the primary effect of the argon atom is to make the transition state geometry less accessible. This has the effect of lowering the cross section for the reactions of the complex. At higher collision energies, the addition of the rare gas atom has two effects. First, it increases the overall size of the target molecule. It can also reduce the amount of energy that is available to the products formed from the O–H–Cl transition species. Since the cross section decreases with increasing available energy, by removing energy from the collision complex the cross section for reactions with Ar–HCl are increased relative to the HCl reactions. These effects are consistent with the reported results of classical trajectory studies of the H + Ar–O_2 reactions [29].

Once the products have been formed, a second set of questions can be asked regarding the effects of the presence of the argon atom on the product state distributions. In general, the presence of the rare gas atom lowers the internal energy of the diatomic

product, and, in the case of the lower energy collisions resulting in reactions (R3) and (R2) more energy is lost from rotation than from vibration. In contrast, in reaction (R1), the presence of the rare gas atom has little effect on the final internal energy of the OH product. The differences between the three reactions are rationalized in terms of the fact that only reaction (R1) proceeds through a long-lived collision complex and the loss of a small fraction of the internal energy of this complex should have a small effect on the overall energy distribution.

Acknowledgements

The author gratefully acknowledges the donors to the Petroleum Research Fund administered by the American Chemical Society, the National Science Foundation CAREER program under grant No. CHE-9732998, and the Ohio State University board of regents for support of this work.

References

[1] W.H. Miller, Annu. Rev. Phys. Chem. 41 (1990) 245.
[2] D.E. Manolopoulos, K. Stark, H.J. Werner, D.W. Arnold, D.N. Neumark, Science 262 (1993) 1852.
[3] G.C. Schatz, J. Phys. Chem. 100 (1996) 12839.
[4] J. Zoval, V.A. Apkarian, J. Phys. Chem. 98 (1994) 7945.
[5] E.R. Bernstein, Annu. Rev. Phys. Chem. 46 (1995) 197.
[6] Y. Hurwitz, P. Stern, R. Naaman, A.B. McCoy, J. Chem. Phys. 106 (1997) 2627.
[7] G. Albert, C. Berg, M. Beyer, U. Achatz, S. Joos, G. Niedner-Schatteberg, V.E. Bondybey, Chem. Phys. Lett. 268 (1997) 235.
[8] J. Zoval, D. Imre, V.A. Apkarian, J. Chem. Phys. 98 (1993) 1.
[9] M.-C. Yang, A.P. Salzberg, B.-C. Chang, C.C. Carter, T.A. Miller, J. Chem. Phys. 98 (1993) 4301.
[10] A.B. McCoy, J. Chem. Phys. 109 (1998) 170.
[11] Atmospheric Ozone as a Climate Gas, General Circulation Model Simulations, W.C. Wang, I.S.A. Isaksen (Eds.), Springer, New York, 1995.
[12] A.B. McCoy, M.W. Lufaso, M. Veneziani, S. Atrill, R. Naaman, J. Chem. Phys. 108 (1998) 9651.
[13] H. Koizumi, G.C. Schatz, M.S. Gordon, J. Chem. Phys. 95 (1991) 6421.
[14] R. Schinke, J. Phys. Chem. 92 (1988) 3195.
[15] W.H. Thompson, W.H. Miller, J. Chem. Phys. 106 (1997) 142.
[16] B. Ramachandran, J. Senekowitsch, R.E. Wyatt, Theochem 388 (1996) 57.
[17] A. Lagana, G. Ochoa de Aspuru, E. Garcia, J. Phys. Chem. 99 (1995) 17139.
[18] L.M. Raff, D.L. Thompson, in: T. Baer (Ed.), Theory of Chemical Reaction Dynamics, CRC Press, Boka Raton, 1985, Vol. 3.
[19] H.R. Mayne, in: R.E. Wyatt, J.Z.H. Zhang (Eds.), Dynamics of Molecules and Chemical Reactions, Marcel Dekker, New York, 1996, pp. 589–616.
[20] G.C. Schatz, Annu. Rev. Phys. Chem. 39 (1988) 317.
[21] J.M. Bowman, G.C. Schatz, Annu. Rev. Phys. Chem. 46 (1995) 169.
[22] J.M. Hutson, J. Chem. Phys. 89 (1988) 4550.
[23] R.W. Bickes Jr., B. Lantzsch, J.P. Toennies, K. Walaschweski, Faraday Discuss. Chem. Soc. 55 (1973) 167.
[24] Z. Ma, K. Liu, L.B. Harding, M. Komotos, G.C. Schatz, J. Chem. Phys. 100 (1994) 8026.
[25] V. Aquilanti, D. Cappelletti, V. Lorent, E. Luzzatti, F. Pirani, J. Phys. Chem. 97 (1993) 2063.
[26] M.I. Lester, W.H. Green, C. Chakravarty, D.C. Clary, in: R. Field, H. Dai (Eds.), Molecular Dynamics and Spectroscopy by SEP, World Scientific Monograph, Singapore, 1995.
[27] M. Allen, D.J. Tildesley, Computer Simulations of Liquids, Clarendon Press, Oxford, 1987.
[28] R.L. LeRoy, J. Phys. Chem. 73 (1969) 4338.
[29] J.M.C. Marques, W. Wang, A.A.C.C. Pais, A.J.C. Varandas, J. Phys. Chem. 100 (1996) 17513.